JOURNAL OF THERMOPHYSICS AND HEAT TRANSFER
Vol. 22, No. 2, April–June 2008

Thermal Transport During Liquid Jet Impingement from a Confined Spinning Nozzle

Muhammad M. Rahman* and Jorge C. Lallave†
University of South Florida, Tampa, Florida 33620

DOI: 10.2514/1.30538

Liquid jet impingement heat transfer from a uniformly heated solid disk of finite thickness and radius is considered in this investigation. The jet nozzle is fitted with a confinement disk that spins with a constant angular velocity about the axis of the nozzle. This arrangement is suitable for microgravity applications in which centrifugal force due to disk rotation can be used to force the fluid over the heated surface. The model covers the entire fluid region (impinging jet and flow spreading out under the confined spinning surface) and solid disk as a conjugate problem. The aim of this paper is to examine how the heat transfer is affected by adding a secondary rotational flow over the jet impingement region. Calculations were done for a range of jet Reynolds numbers (500–1500), rotational rates of 0–750 rpm or Ekman numbers ($7.08 \times 10^{-5} - \infty$), nozzle-to-target spacings ($\beta = 0.25$–5.0), and disk-thicknesses-to-nozzle-diameter ratios ($b/d_n = 0.25$–1.67). Calculations were done for ammonia (NH_3), water (H_2O), flouroinert (FC-77), and oil (MIL-7808), which were used as working fluids, and copper, silver, constantan, and silicon, which were used as solid disk materials. This provided a Prandtl number range of 1.29–124.44 and a solid-to-fluid thermal conductivity ratio of 36.91–2222. Plate materials with higher thermal conductivity maintained a more uniform and lower interface temperature distribution. A higher Reynolds number increased the local heat transfer coefficient over the entire interface. The rotational rate increased the local heat transfer coefficient under most conditions.

Nomenclature

b	=	disk thickness, m
C_p	=	specific heat, J/kg · K
d_n	=	diameter of nozzle, m
Ek	=	Ekman number, $\nu/(4 \cdot \Omega \cdot r_d^2)$
g	=	acceleration due to gravity, m/s^2
H_n	=	height of the nozzle from the plate, m
h	=	heat transfer coefficient, W/m^{2}K, $q_{\text{int}}/(T_{\text{int}} - T_j)$
k	=	thermal conductivity, W/m K
Nu	=	Nusselt number, $(h \cdot d_n)/k_f$
Nu_{av}	=	average Nusselt number for the entire surface, $(h_{\text{av}} \cdot d_n)/k_f$
nr	=	number of elements in radial direction
nz	=	number of elements in axial direction
Pr	=	Prandtl number, ν_f/α_f
p	=	pressure, Pa
q	=	heat flux, W/m^2
Re	=	Reynolds number, $(V_J \cdot d_n)/\nu_f$
r	=	radial coordinate, m
r_d	=	disk radius, m
T	=	temperature, K
$\bar{T}_{\text{int}}$	=	average interface temperature, K, $\frac{2}{r_d^2}\int_0^{r_d} T_{\text{int}} r\,\mathrm{d}r$
V_j	=	jet velocity, m/s
$V_{r,z,\theta}$	=	velocity component in the r, z, and θ directions, m/s
z	=	axial coordinate, m
α	=	thermal diffusivity, m^2/s
β	=	dimensionless nozzle-to-target spacing, H_n/d_n
ε	=	thermal conductivity ratio, k_s/k_f
Θ	=	dimensionless temperature, $2 \cdot k_f \cdot (T_{\text{int}} - T_J)/(q \cdot d_n)$
θ	=	angular coordinate, rad
μ	=	dynamic viscosity, kg/m · s
ν	=	kinematic viscosity, m^2/s
ρ	=	density, kg/m^3
Ω	=	angular velocity, rad/s

Subscripts

atm	=	ambient
av	=	average
f	=	fluid
int	=	solid–fluid interface
j	=	jet or inlet
n	=	nozzle
s	=	solid

Received 18 February 2007; revision received 4 September 2007; accepted for publication 15 September 2007.

*Professor, Department of Mechanical Engineering, 4202 E. Fowler Avenue, Engineering Building II 118.

†Graduate Student, Department of Mechanical Engineering, 4202 E. Fowler Avenue, Engineering Building II 118.

Introduction

COOLING, heating, and drying processes are often used in industry. In many applications, a high heat transfer rate and/or a short processing time is required to preserve product quality and reliability. A technique that can be used for cooling or heating at high rates is the liquid jet impingement. Processes like turbine blade cooling, annealing of metal, and tempering of glass can use this technique. Jet impingement is also being adapted for the cooling of electronic components.

To achieve a reliable cooling system design with an impinging jet, one has to choose an appropriate jet configuration and surrounding geometry. It is necessary to understand that the heat transfer rate from an impinging jet onto a surface is a complex function of many parameters such as flow rate, working fluid properties, nozzle structure and orientation, nozzle-to-target spacing, and displacement from the stagnation point. Even though a number of publications have considered the effect of these parameters on the heat transfer rate, the combination of the rotation and liquid jet impingement cooling effects have not been thoroughly investigated. The data are typically restricted to either the cooling of a stationary disk by jet impingement or cooling by pure rotation. Additionally, most of these works deal with average heat transfer measurements rather than local distributions. The liquid jet considered in this study is axisymmetric and submerged, with the jet issuing into a region containing the same liquid. The jet nozzle is attached to a spinning confinement disk parallel to the impingement surface with a separation distance of H_n.

Heat and mass transfer characteristics of an impinging axisymmetric jet issuing from a circular nozzle have been studied by Scholtz and Trass [1]. The theoretical and experimental findings are well correlated in the stagnation flow and in the wall jet regions. Nakoryakov et al. [2] studied, both theoretically and experimentally, the hydrodynamics and mass transfer of a liquid jet impinging onto a horizontal plate. Simple formulas were developed for the calculation of the friction factor, liquid layer thickness, surface velocity, and convection heat transfer coefficient at stagnation point as a function of discharge parameters. Womac et al. [3] presented correlating equations for the heat transfer coefficient for the cooling of discrete heat sources by liquid jet impingement. Liu et al. [4] presented an analytical and experimental investigation for jet impingement cooling of uniformly heated surfaces to determine the local Nusselt number from the stagnation point to radii up to 40 diameters. Ma et al. [5] reported experimental measurements for the local heat transfer coefficient during impingement of a circular jet perpendicular to a target plate. Both confined and freejet configurations were used. Ethylene glycol and transformer oil were used as working fluids. Garimella and Nenaydykh [6], Fitzgerald and Garimella [7], Li et al. [8], and Rahman et al. [9] all considered a confining top plate such as the one used in the present study for a submerged liquid jet. However, no rotation was used. Their studies covered a number of working fluids including flouroinert (FC-77) and ammonia (NH_3) at different volumetric flow rates. In addition, Garimella and Rice [10] presented experimental results for the distribution of the local heat transfer coefficient during confined submerged liquid jet impingement with FC-77 as the working fluid. Morris and Garimella [11] computationally investigated the flowfields in the orifice and the confinement regions of a normally impinging, axisymmetric, confined and submerged liquid jet. Li and Garimella [12] experimentally investigated the influence of fluid thermophysical properties on the heat transfer from confined and submerged impinging jets. Generalized correlations for heat transfer were proposed based on their results. Ichimiya and Yamada [13] studied the heat transfer and flow characteristics of a single circular laminar impinging jet including the buoyancy effect in a narrow space with a confining wall. Temperature distribution and velocity vectors in the space were obtained numerically. Dano et al. [14] investigated the flow and heat transfer characteristics of the confined jet array impingement with crossflow. Digital particle image velocimetry and flow visualization were used to determine the flow characteristics. Rahman and Mukka [15] developed a numerical model for the conjugate heat transfer during the vertical impingement of a two-dimensional (slot) submerged confined liquid jet using liquid ammonia as the working fluid.

The jet impingement on a rotating disk adds more complexity to the flowfield. Carper and Deffenbaugh [16] conducted experiments to determine the average heat transfer coefficients for the rotating solid–fluid interface, with uniform temperature, cooled by a single liquid jet of oil impinging normal to the rotating disk. Their tests were conducted over a range of jet flow rates and disk rotational speeds with various combinations of jet nozzle and disk diameters. Carper et al. [17] conducted experiments to determine the average heat transfer coefficient for a rotating disk with a uniform temperature cooled by a single liquid jet of oil impinging normal to the surface. They documented the effects of the rotational Reynolds number on the average Nusselt number for various jet Reynolds numbers. A nondimensional correlation was given in terms of jet and rotational Reynolds numbers. Metzger et al. [18] employed liquid crystal for mapping local heat transfer distributions on a rotating disk with jet impingement.

Thomas et al. [19] measured the film thickness across a stationary and rotating horizontal disk using the capacitance technique, in which the liquid was delivered to the disk by a controlled impinging jet. Rahman and Faghri [20] presented the results of a numerical simulation of the flowfield and the associated heat transfer coefficient for the free surface flow of a thin liquid film adjacent to a horizontal rotating disk. The computation was performed for different flow rates and rotational velocities using a three-dimensional boundary-fitted coordinate system. Rahman and Faghri [21] analyzed the processes of heating and evaporation in a thin liquid film adjacent to a horizontal disk rotating about a vertical axis at a constant angular velocity. The fluid emanated axisymmetrically from a source at the center of the disk and was carried downstream by inertial and centrifugal forces.

Saniei et al. [22] investigated the heat transfer coefficients from a rotating disk with jet impingement at its geometric center. The jet was placed perpendicular to the disk surface at four different distances from the center of the disk. Saniei and Yan [23] presented local heat transfer measurements for a rotating disk cooled with an impinging air jet. Several important factors such as rotational Reynolds number, jet Reynolds number, jet-to-disk spacing, and the location of the jet center relative to the disk center were examined. Rahman [24] presented a theoretical analysis of the process of gas absorption to a thin liquid film formed by the impingement of a confined liquid jet at the center of a horizontal rotating disk and the subsequent radial spreading of liquid along the surface of the disk.

Hung and Shieh [25] reported experimental measurements of the heat transfer characteristics of jet impingement onto a horizontally rotating ceramic-based multichip disk. The chip temperature distributions along with local and average Nusselt numbers were presented. Kang and Yoo [26] carried out an experimental study using hot-wire anemometry to investigate the turbulence characteristics of the three-dimensional boundary layer on a rotating disk with jet impingement at its center. Shevchuk et al. [27] presented an approximate analytical solution using an integral method for jet impingement heat transfer over a rotating disk. Iacovides et al. [28] reported an experimental study of impingement cooling in a rotating passage of a semicylindrical cross section. Cooling fluid was injected from a row of five jet holes along the centerline of the flat surface of the passage and impinged the concave surface.

From this review of the current literature, it is clear that there is no heat transfer data available for jet impingement with a rotating confinement disk. The intent of this research is to study conjugate heat transfer with a steady flow over a solid stationary disk confined by a rotating disk under five different flow rates or jet Reynolds numbers, seven spinning rates or Ekman numbers, six different disk thicknesses, and eight nozzle-to-target spacing ratios. A broad range of Prandtl number was covered with the use of four working fluids, namely, water, ammonia, FC-77, and MIL-7808. The thermal conductivity effect was studied with the implementation of four different disk materials: copper, silicon, silver, and constantan. The results offer a better understanding of the fluid mechanics and heat transfer behavior of liquid jet impingement under an insulated spinning wall condition. Even though no new numerical technique has been developed, results obtained in the present investigation are entirely new. The numerical results showing the quantitative effects of different parameters as well as the correlation for an average Nusselt number will be practical guides for the enhancement of heat or mass transfer under microgravity.

Analysis and Computation

A schematic of the physical problem is shown in Fig. 1. An axisymmetric liquid jet is discharged through a nozzle and impinges at the center of a solid uniformly heated circular disk. The top plate acts as an insulated confinement surface subjected to a uniform rotational velocity. Heat is conducted through the disk and convected out to the fluid adjacent to the top surface of the stationary disk as shown in Fig. 1. The present study considered an incompressible, Newtonian, and axisymmetric flow under a steady-state condition. The variation of fluid properties with local temperature was taken into account. Because of the rotational symmetry of the problem, the $\partial/\partial\theta$ terms could be omitted. The equations describing the conservation of mass, momentum (r, θ, and z directions, respectively), and energy can be written as seen in Burmeister [29]:

$$\frac{1}{r}\frac{\partial}{\partial r}(\rho_f r V_r) + \frac{\partial}{\partial z}(\rho_f V_z) = 0 \tag{1}$$

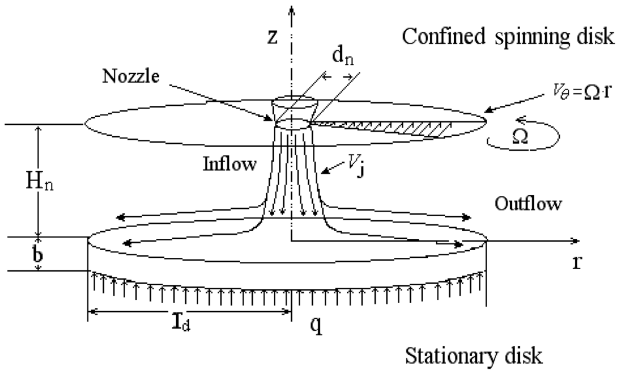

Fig. 1 Three-dimensional schematic of an axisymmetric confined spinning disk liquid jet impingement on a uniformly heated disk.

$$\rho_f\left(V_r\frac{\partial V_r}{\partial r}+V_z\frac{\partial V_r}{\partial z}-\frac{V_\theta^2}{r}\right)=-\frac{\partial p}{\partial r}+\frac{1}{r}\frac{\partial}{\partial r}\left[\frac{2}{3}\cdot\mu_f r\left(2\frac{\partial V_r}{\partial r}-\frac{V_r}{r}-\frac{\partial V_z}{\partial z}\right)\right]+\frac{\partial}{\partial z}\left[\mu_f\left(\frac{\partial V_r}{\partial z}+\frac{\partial V_z}{\partial r}\right)\right]+\frac{2}{3}\cdot\frac{\mu_f}{r}\left(\frac{\partial V_r}{\partial r}+\frac{\partial V_z}{\partial z}-\frac{2\cdot V_r}{r}\right) \tag{2}$$

$$\rho_f\left(V_r\frac{\partial V_\theta}{\partial r}+V_z\frac{\partial V_\theta}{\partial z}+\frac{V_rV_\theta}{r}\right)=\frac{1}{r^2}\frac{\partial}{\partial r}\left\{r^2\mu_f\left[r\frac{\partial}{\partial r}\left(\frac{V_\theta}{r}\right)\right]\right\}+\frac{\partial}{\partial z}\left[\mu_f\left(\frac{\partial V_\theta}{\partial z}\right)\right] \tag{3}$$

$$\rho_f\left(V_r\frac{\partial V_z}{\partial r}+V_z\frac{\partial V_z}{\partial z}\right)=-\rho_f g-\frac{\partial p}{\partial z}+\frac{1}{r}\frac{\partial}{\partial r}\left[r\mu_f\left(\frac{\partial V_r}{\partial z}+\frac{\partial V_z}{\partial r}\right)\right]+\frac{\partial}{\partial z}\left[\frac{2}{3}\mu_f\left(2\frac{\partial V_z}{\partial z}-\frac{V_r}{r}-\frac{\partial V_r}{\partial r}\right)\right] \tag{4}$$

$$\rho_f\left(V_r\frac{\partial(Cp_fT_f)}{\partial r}+V_z\frac{\partial(Cp_fT_f)}{\partial z}\right)=\left[\frac{1}{r}\frac{\partial}{\partial r}\left(k_fr\frac{\partial T_f}{\partial r}\right)+\frac{\partial}{\partial z}\left(k_f\frac{\partial T_f}{\partial r}\right)\right]+2\cdot\mu_f\left[\left(\frac{\partial V_r}{\partial r}\right)^2+\left(\frac{V_r}{r}\right)^2+\left(\frac{\partial V_z}{\partial z}\right)^2+\frac{1}{2}\left(\frac{\partial V_\theta}{\partial r}-\frac{V_\theta}{r}\right)^2+\frac{1}{2}\left(\frac{\partial V_\theta}{\partial z}\right)^2+\frac{1}{2}\left(\frac{\partial V_r}{\partial z}+\frac{\partial V_z}{\partial r}\right)^2-\frac{1}{3}\left(\frac{\partial V_r}{\partial r}+\frac{V_r}{r}+\frac{\partial V_z}{\partial z}\right)^2\right] \tag{5}$$

The variation of the thermal conductivity of solids with temperature was not significant. Therefore, the conservation of energy inside the solid can be characterized by the following equation:

$$\frac{\partial^2 T_s}{\partial r^2}+\frac{1}{r}\left(\frac{\partial T_s}{\partial r}\right)+\frac{\partial^2 T_s}{\partial z^2}=0 \tag{6}$$

The following boundary conditions were used to complete the physical problem formulation.

$$\text{At } r=0,\qquad -b\le z\le 0:\ \frac{\partial T_s}{\partial r}=0 \tag{7}$$

$$\text{At } r=0,\qquad 0\le z\le H_n:\ V_\theta=V_r=0,\ \frac{\partial V_z}{\partial r}=0,\ \frac{\partial T_f}{\partial r}=0 \tag{8}$$

$$\text{At } r=r_d,\qquad -b\le z\le 0:\ \frac{\partial T_s}{\partial r}=0 \tag{9}$$

$$\text{At } r=r_d,\qquad 0\le z\le H_n:\ p=p_{\text{atm}} \tag{10}$$

$$\text{At } z=-b,\qquad 0\le r\le r_d:\ -k_s\frac{\partial T_s}{\partial z}=q \tag{11}$$

$$\text{At } z=0,\qquad 0\le r\le r_d:\ V_r=V_z=V_\theta=0,\quad T_f=T_s,\quad k_s\frac{\partial T_s}{\partial z}=k_f\frac{\partial T_f}{\partial z} \tag{12}$$

$$\text{At } z=H_n,\qquad 0\le r\le \frac{d_n}{2}:\ V_z=-V_j,\quad V_r=V_\theta=0,\quad T_f=T_j \tag{13}$$

$$\text{At } z=H_n,\qquad \frac{d_n}{2}\le r\le r_d:\ V_\theta=\Omega\cdot r,\quad V_r=V_z=0,\quad \frac{\partial T_f}{\partial z}=0 \tag{14}$$

The local and average heat transfer coefficients can be defined as

$$h=\frac{q}{(T_{\text{int}}-T_J)} \tag{15}$$

$$h_{\text{av}}=\frac{2}{r_d^2\cdot(\bar{T}_{\text{int}}-T_J)}\int_0^{r_d}hr(T_{\text{int}}-T_J)\,\mathrm{d}r \tag{16}$$

where $\bar{T}_{\text{int}}$ is the average temperature at the solid–liquid interface. The average temperature was calculated by taking the area-weighted average of the local interface temperature. The local and average Nusselt numbers are calculated according to the following expressions:

$$Nu=\frac{h\cdot d_n}{k_f} \tag{17}$$

$$Nu_{\text{av}}=\frac{h_{\text{av}}\cdot d_n}{k_f} \tag{18}$$

The characteristics of the flow are controlled by three major physical parameters: the Reynolds number, $Re_J=V_Jd_n/\nu_f$; the dimensionless nozzle-to-target spacing ratio, $\beta=H_n/d_n$; and the Ekman number, $Ek=\nu_f/4\cdot\Omega r_d^2$. The bottom disk remains stationary while the top disk rotates at a uniform angular velocity. The values of the Reynolds number was limited to a maximum of 1500 to stay within the laminar region. The nozzle opening and the solid wafer disk have a radius of 0.6 and 6.0 mm, respectively. The heat flux (q) was kept constant at a value of 250 kW/m^2. The incoming fluid jet temperature (T_J) was 310 K for water and FC-77, 303 K for ammonia (at a pressure of 20 bars), and 373 K for MIL-7808. The thickness of the disk was varied over the following values: 0.3, 0.6, 0.9, 1.2, 1.5, and 2.0 mm. The jet impingement height, or the distance between the nozzle and disk, was set at the following values: 3×10^{-4}, 6×10^{-4}, 9×10^{-4}, 1.2×10^{-3}, 2.4×10^{-3}, 3.6×10^{-3}, 4.8×10^{-3}, and 6×10^{-3} m. The spinning rate (Ω) was varied from 0 to 78.54 rad/s or 0 to 750 rpm. The flow rate was varied from 3.78×10^{-7} to 1.13×10^{-6} m^3/s. The ranges for the Reynolds number and Ekman number were $Re=500$–1500 and $Ek=7.08\times10^{-5}$–∞. The possibility of getting into turbulent flow due to disk rotation was checked, using the laminar–turbulent transition criterion used by Popiel and Boguslawski [30] and Vanyo

[31]. All runs used in the paper checked out to be laminar. The simulation was carried out for a number of disk materials, namely constantan, copper, silicon, and silver.

The properties of solid materials were obtained from Özisik [32]. Fluid properties for H_2O, NH_3, MIL-7808, and FC-77 were obtained from Bejan [33], the Brady vendor, and 3M Specialty Fluids, respectively. The properties of the aforementioned fluids were correlated according to the following equations. For water between 300 K $< T <$ 411 K, $Cp_f = 9.5 \times 10^{-3}T^2 - 5.9299T + 5098.1$, $k_f = -7.0 \times 10^{-6}T^2 + 5.8 \times 10^{-3}T - 0.4765$, $\rho_f = -2.7 \times 10^{-3}T^2 + 1.3104T + 848.07$, and $\ell_n(\mu_f) = -3.27017 - 0.0131T$. For ammonia between 273.15 K $< T <$ 370 K, $Cp_f = 0.083T^2 - 40.489T + 9468$, $k_f = 1.159 - 2.30 \times 10^{-3}T$, $\rho_f = 579.81 + 1.6858T - 0.0054T^2$, and $\ell_n(\mu_f) = -5.33914 - 0.0115T$. For MIL-7808 between 303 K $< T <$ 470 K, $Cp_f = 903.8 + 3.332T$, $k_f = 0.18 - 1 \times 10^{-4}T$, $\rho_f = 1181 - 0.708T$, and $\ell_n(\mu_f) = 3.2436 - 0.0229T$. For FC-77 between 273 K $< T <$ 380 K, $Cp_f = 589.2 + 1.554T$, $k_f = 0.0869 - 8 \times 10^{-5}T$, $\rho_f = 2507.2 - 2.45T$, and $\ell_n(\mu_f) = -2.38271 - 0.0145T$. In these correlations, the absolute temperature T was used in K.

The governing Eqs. (1–6) along with the boundary conditions (7–14) were solved using the Galerkin finite element method as demonstrated by Fletcher [34]. Four node quadrilateral elements were used. In each element, the velocity, pressure, and temperature fields were approximated, which led to a set of equations that defined the continuum. The number of elements required for accurate results was determined from a grid independence study. An unstructured grid was used in which the size of the elements near the solid–fluid interface was made smaller to adequately capture large variations in velocity and temperature in that region. The solution of the resulting nonlinear differential equations was carried out using the Newton–Raphson method. Because of the nonlinear nature of the governing transport equations, an iterative procedure was used to arrive at the solution for the velocity and temperature fields. The solution was considered converged when the field value did not change from one iteration to the next and the sum of the residuals for all the dependent variables was less than a predefined tolerance value, in this case, 10^{-6}.

Results and Discussion

This section describes the heat transfer characteristics of a confined liquid jet impingement under a spinning confinement disk. Several grids or combinations of number of elements were used to determine the accuracy of the numerical solution. Dimensionless solid–fluid interface temperatures at the heated plate for several grids are plotted in Fig. 2. The numerical solution becomes grid independent when the number of divisions equal to 40×70 in the axial (z) and radial (r) directions, respectively, is used. Numerical results for a 40×70 grid gave almost identical results compared with

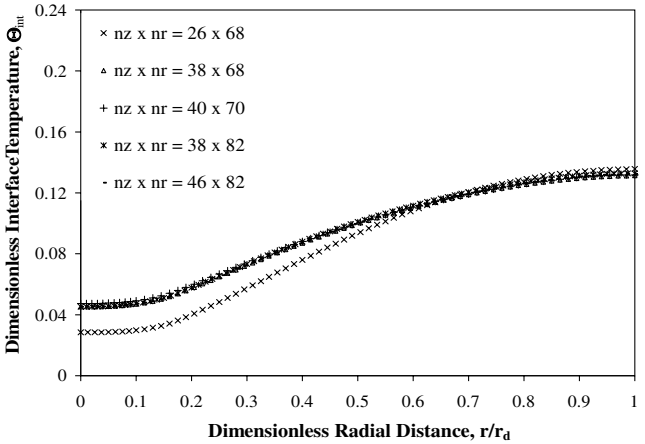

Fig. 2 Dimensionless interface temperature distributions for a different number of elements in r and z directions ($Re = 1000$, $b = 0.3$ mm, $d_n = 0.12$ mm, $Ek = 1.06 \times 10^{-3}$, $\beta = 2.0$).

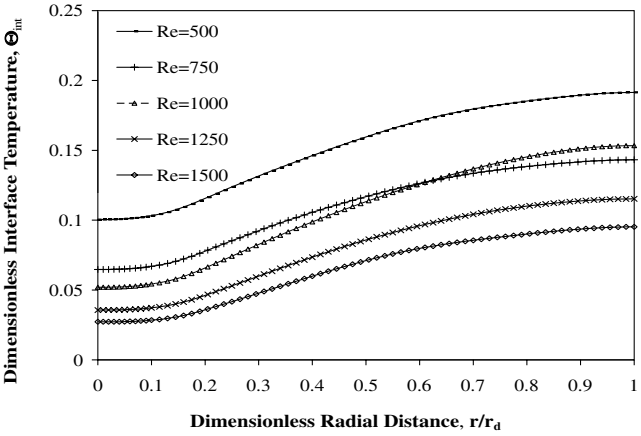

Fig. 3 Dimensionless interface temperature distributions for a silicon disk with water as the cooling fluid for different Reynolds numbers ($Ek = 4.25 \times 10^{-4}$, $\beta = 2.0$, $b/d_n = 0.25$).

38×82 and 46×82 grids for an impingement height (H_n) equal to 0.24 cm. The average difference was 0.69%. Therefore, all further computations were carried out using 40×70 elements. The size of the elements varied with a denser distribution at the solid–fluid interface and at the nozzle axis. Scaling ratios of 1.5 and 1.62 were used in the radial and axial directions, respectively.

Figure 3 shows the variation of the solid–fluid dimensionless interface temperature for different Reynolds numbers under a low rotational rate ($Ek = 4.25 \times 10^{-4}$). The plots in Fig. 3 reveal that dimensionless interface temperature decreases with jet velocity (or Reynolds number). At any Reynolds number, the dimensionless interface temperature has the lowest value at the stagnation point (underneath the center of the axial opening) and increases radially downstream reaching the highest value at the end of the disk. This is due to the development of the thermal boundary layer as the fluid moves downstream from the center of the disk. The thickness of the thermal boundary layer increases with the radius and causes the interface temperature to increase. The increment of the dimensionless interface temperature coincides with the thickening of the thermal boundary layer. It may be noted, however, that due to spinning streamlines are not aligned along the disk radius, rather the fluid moves at an angle based on the rate of rotation. A lower interface temperature distribution at $Re = 750$ is attained in comparison with $Re = 1000$ for the dimensionless radial distance, $r/r_d > 0.6$. This is due to the fact that the tangential velocity from the top plate penetrates into the thermal boundary-layer thickness adjacent to the heated stationary disk. This effect remains stronger when the momentum of the jet fluid is lower. At higher Reynolds numbers (i.e., $Re \geq 1000$), the jet fluid momentum overcomes the tangential velocity effects and increases the dimensionless interface temperature.

Figure 4 presents the local Nusselt number distributions along the solid–fluid interface for different Reynolds numbers for the same rotational rate ($Ek = 4.25 \times 10^{-4}$). All local Nusselt number distributions are half-bell shaped with a peak at the stagnation point. Figures 3 and 4 confirm to us how an increasing Reynolds number contributes to a more effective cooling. Similar profiles have been documented by Garimella and Nenaydykh [6] and Ma et al. [35]. The positive influence of the spinning of the confinement disk can be observed particularly at $Re = 750$, at which point the Nusselt number at $r/r_d > 0.6$ becomes higher in comparison with that of the Reynolds number of 1000.

Figure 5 plots the average Nusselt number as a function of the Reynolds number for low, intermediate, and high Ekman numbers. It may be noted that the average Nusselt number increases with the Reynolds number. As the flow rate (or Reynolds number) increases, the magnitude of fluid velocity near the solid–fluid interface that controls the convective heat transfer rate increases. Furthermore, at a particular Reynolds number, the Nusselt number decreases with the Ekman number (or gradually increases with the increment of disk

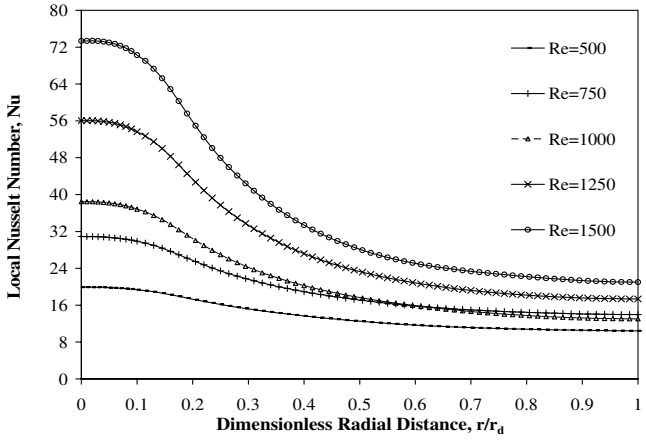

Fig. 4 Local Nusselt number distributions for a silicon disk with water as the cooling fluid for different Reynolds numbers ($Ek = 4.25 \times 10^{-4}$, $\beta = 2.0$, $b/d_n = 0.25$).

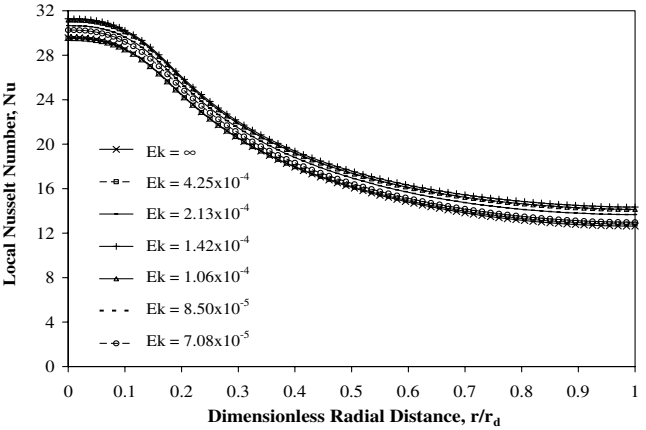

Fig. 6 Local Nusselt number distributions for a silicon disk with water as the cooling fluid at different Ekman numbers ($Re = 750$, $\beta = 3.0$, $b/d_n = 0.25$).

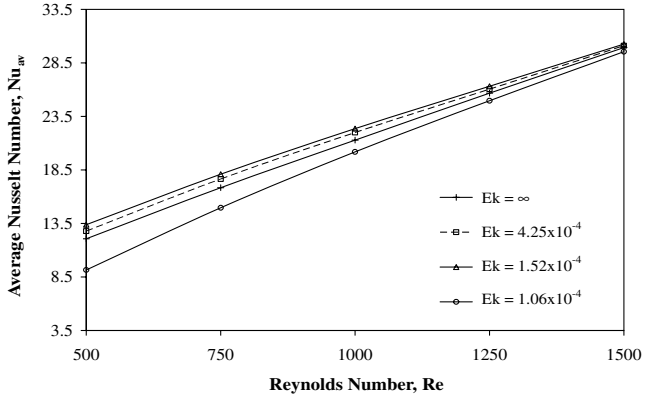

Fig. 5 Average Nusselt number variations with Reynolds number at different Ekman numbers for a silicon disk with water as the cooling fluid ($\beta = 2.0$, $b/d_n = 0.25$).

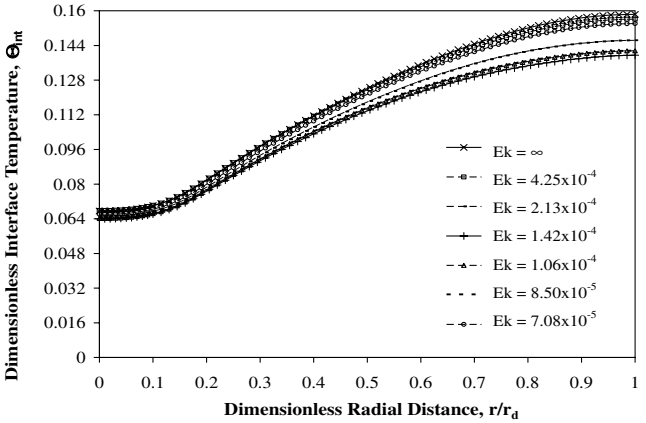

Fig. 7 Dimensionless interface temperature distributions for a silicon disk with water as the cooling fluid at different Ekman numbers ($Re = 750$, $\beta = 3.0$, $b/d_n = 0.25$).

spinning rate). This behavior confirms the positive influence of the rotational rate on the average Nusselt number down to $Ek = 1.52 \times 10^{-4}$ that corresponds to a spinning rate of 350 rpm. However, at $Ek = 1.06 \times 10^{-4}$ (a spinning rate of 500 rpm) the average Nusselt number is lower than the stationary disk ($Ek = \infty$). At a high spinning rate, the thermal boundary-layer thickness increases due to suction created by the spinning motion of the confinement plate. Therefore, the heat transfer coefficient decreases compared with the stationary disk; the average Nusselt numbers decreases by 39% at $Re = 750$ and by 2% at $Re = 1500$. It may also be noticed that the average Nusselt number plots get closer to each other as the Reynolds number increases, indicating that the curves will intersect at higher Reynolds numbers. These intersections indicate the presence of a liquid jet momentum dominated region at higher Reynolds numbers. From the numerical results, it was observed that the heat transfer is dominated by impingement when $Re \cdot Ek > 0.11$ and dominated by disk rotation when $Re \cdot Ek < 0.07$. In between these limits, both of these effects play important roles in determining the variations of the average Nusselt number. This type of behavior is consistent with the experimental results of Brodersen et al. [36], in which the ratio of jet and rotational Reynolds numbers was used to characterize the flow regime.

The rotational rate effects on the local Nusselt number and solid–fluid dimensionless interface temperature are illustrated in Figs. 6 and 7 for a Reynolds number of 750 and a dimensionless nozzle-to-target spacing (β) equal to 3. It may be noted that the rotational effect increases the local Nusselt number and generates a lower temperature over the entire solid–fluid interface with somewhat less intensity in comparison with the Reynolds number effect. Figure 7 shows that dimensionless interface temperature decreases with the increment of the rotational rate; as the Ekman number decreases from ∞ to 1.42×10^{-4}, the local Nusselt number increases by an average 5.56% in Fig. 6 and the dimensionless interface temperature decreases by an average 2.32% in Fig. 7 under a Reynolds number of 750. The enhancement of the Nusselt number due to rotation is primarily caused by the enhancement of local fluid velocity adjacent to the heated disk surface. The tangential velocity due to rotation combined with axial and radial velocities due to jet momentum results in an increased magnitude of velocity vector starting from the center of the disk.

The effects of disk thickness variation on the solid–fluid dimensionless interface temperature and local Nusselt number are shown in Figs. 8 and 9, respectively. In these plots, silicon has been used as the disk material and water as the cooling fluid for a Reynolds number of 1500 and rotational rate of 350 rpm ($Ek = 1.52 \times 10^{-4}$). The dimensionless solid–fluid interface temperature increases from the impingement region all the way to the end of the disk. When the temperature is lower in the stagnation region, a higher outflow temperature is obtained. This is quite expected because the total heat transferred to the disk as well as the fluid flow rates are the same for all the cases. It may be noted that the disk thickness variation results intersect with each other around the dimensionless radial distance of $r/r_d = 0.65$. Thicker disks generate a more uniform dimensionless interface temperature due to the larger radial conduction within the disk. The local Nusselt number plots in Fig. 9 change significantly with the variation of disk thickness. In all cases, it is evident that the Nusselt number is sensitive to the solid thickness especially at smaller radii where higher Nusselt number are obtained due to the rapid development of thermal boundary layer.

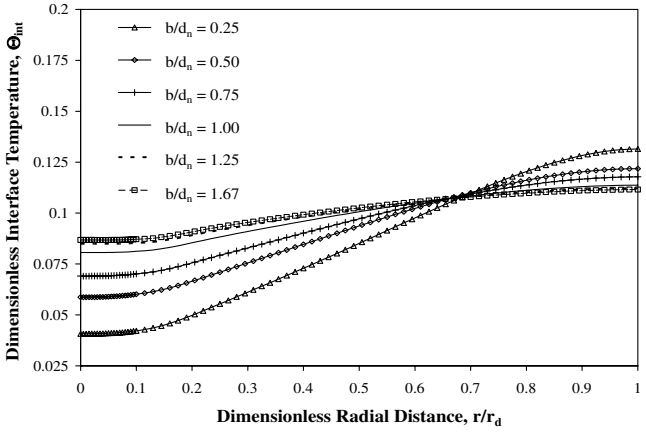

Fig. 8 Dimensionless interface temperature distributions for different silicon disk thicknesses with water as the cooling fluid ($Re = 1500$, $\mathrm{Ek} = 1.52 \times 10^{-4}$, $\beta = 2.0$).

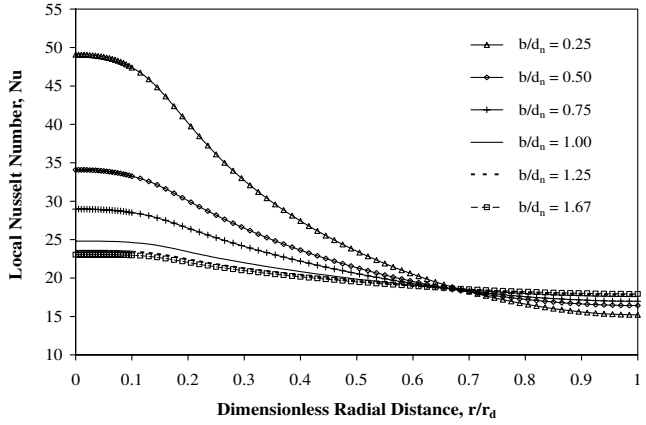

Fig. 9 Local Nusselt number distributions for different silicon disk thicknesses with water as the cooling fluid ($Re = 1500, Ek = 1.52 \times 10^{-4}$, $\beta = 2.0$).

Eight different nozzle-to-target spacing ratios (β) from 0.25 to 5 were modeled for water as the coolant and silicon as the disk material. The effects of nozzle-to-target spacing on the local Nusselt number and dimensionless interface temperature at a spinning rate of 125 rpm or ($Ek = 4.25 \times 10^{-4}$) and Reynolds number of 750 are shown in Figs. 10 and 11. It may be noticed that the impingement height quite significantly affects the Nusselt number distribution, particularly at the stagnation region. It may be noticed that a very high local Nusselt

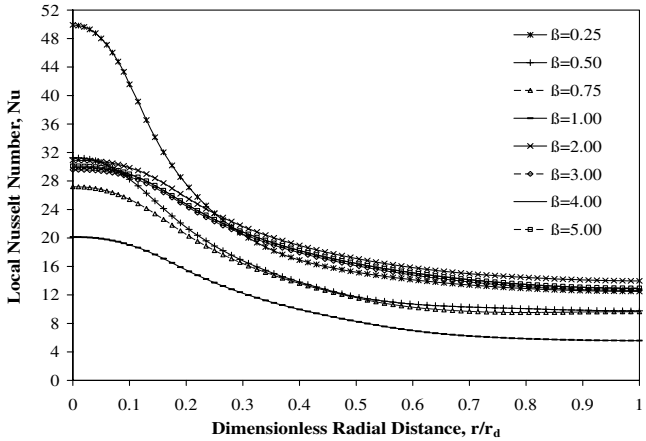

Fig. 10 Local Nusselt number distributions for a silicon disk with water as the cooling fluid for different nozzle-to-target spacings ($Re = 750$, $Ek = 4.25 \times 10^{-4}$, $b/d_n = 0.25$).

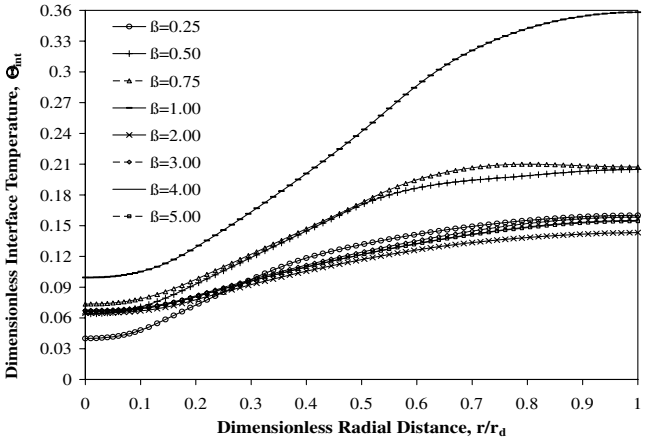

Fig. 11 Dimensionless interface temperature distributions for a silicon disk with water as the cooling fluid for different nozzle-to-target spacings ($Re = 750$, $Ek = 4.25 \times 10^{-4}$, $b/d_n = 0.25$).

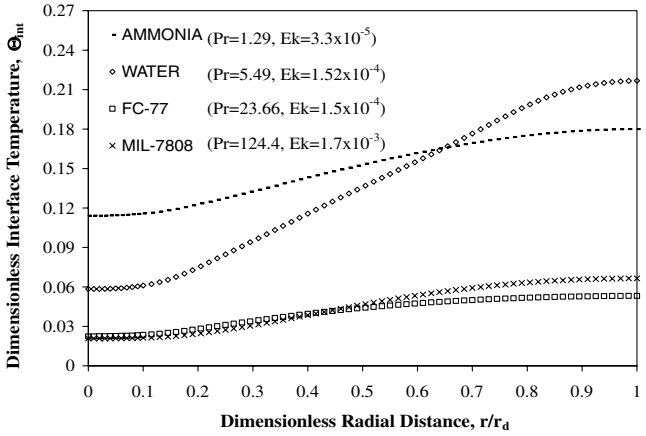

Fig. 12 Dimensionless interface temperature distributions for different cooling fluids with silicon as the disk material ($Re = 1000$, $\beta = 2.0$, $b/d_n = 0.25$).

number at the stagnation region is obtained when the nozzle is brought very close to the heated disk ($\beta = 0.25$). The spinning motion of the confinement disk really penetrates through the thermal boundary layer adjacent to the heated stationary disk and provides a larger fluid velocity and, therefore, a larger rate of convective heat transfer. As the nozzle is moved away from the disk ($\beta = 0.25$–1), the local Nusselt number decreases. This is due to the smaller effect of the rotational velocity of the confinement disk. Also, as the spacing is increased, the jet fluid needs to travel a larger distance through the existing fluid column between the target and confinement disks and thereby loses its momentum. The minimum stagnation Nusselt number is seen for $\beta = 1$, and also the shape of the curve somewhat changes. The nozzle-to-target ratio of $\beta = 2.0$ generates an optimal mix of the impinging jet flow with the rotationally induced flow, resulting in a higher heat transfer rate. There is only a small change in Nusselt number values at spacings greater than $\beta = 2$. This observation is in line with the previous study by Hung and Lin [37] for a confined jet impingement with a stationary disk.

Figure 12 compares the dimensionless solid–fluid interface temperature results of the present working fluid (water) with three other coolants that have been considered in previous thermal management studies, namely ammonia (NH_3), flouroinert (FC-77), and oil (MIL-7808) under a Reynolds number of 1000. Even though the rotational rate (Ω) for the top confining wall was set at 350 rpm, the variation of the Ekman number occurred because the density (ρ) and dynamic viscosity (μ) are different for each fluid. The interface temperature distribution of Fig. 12 shows similar results for FC-77 and MIL-7808. It may be noticed that both ammonia and water

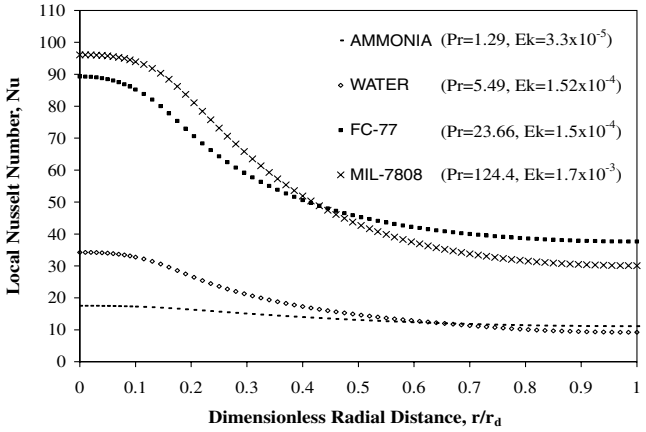

Fig. 13 Local Nusselt number distributions for different cooling fluids with silicon as the disk material ($Re = 1000$, $\beta = 2.0$, $b/d_n = 0.25$).

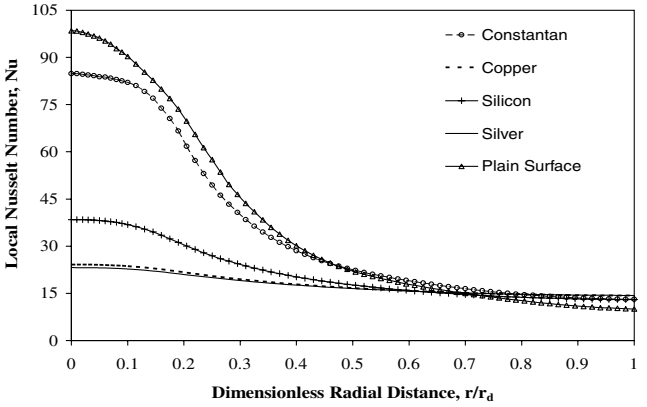

Fig. 15 Local Nusselt number distributions for different solid materials with water as the cooling fluid ($Re = 1000$, $Ek = 4.25 \times 10^{-4}$, $\beta = 2.0$, $b/d_n = 0.25$).

present a higher dimensionless interface temperature distribution in comparison with MIL-7808 and FC-77. Water shows a larger variation of the dimensionless interface temperature along the radius of the disk. The water and ammonia curves intersect at a dimensionless radial distance of $r/r_d = 0.65$. Figure 13 shows the corresponding local Nusselt number distributions. It may be noticed that MIL-7808 presents the highest local Nusselt number values in comparison with water, NH_3, and FC-77 for a dimensionless radial distance, $r/r_d < 0.45$. Only FC-77 exhibits a higher heat removal rate beyond this point. MIL-7808 shows the largest variation of the local Nusselt number, primarily because of its large variation of viscosity with temperature. Ammonia provides the lowest Nusselt number because of its small Prandtl number. Higher Prandtl number fluids lead to a thinner thermal boundary layer and more effective heat removal rate at the interface. Present working fluid results are in agreement with the findings of Li et al. [8], in which a larger Prandtl number corresponded to a higher recovery factor. Thus, different Prandtl numbers represent different thermal boundary-layer thicknesses and different heat generations by viscous dissipation of the fluids.

The dimensionless solid–fluid interface temperature and local Nusselt number distribution plots as a function of a dimensionless radial distance (r/r_d) measured from the axisymmetric impingement axis for different solid materials with water as the working fluid are plotted in Figs. 14 and 15, respectively. The numerical simulation was carried out for a set of materials, namely, copper, silver, constantan, and silicon, having different thermophysical properties at a Reynolds number of 1000 and Ekman number of 4.25×10^{-4}. Results for a plain surface (zero thickness of the disk) are also plotted to identify the extent of conjugate effects. The temperature distribution plots reveal how the thermal conductivity of the solid affects the heat flux distribution that controls the local interface temperature. It may be noted that the plain surface has the lowest temperature at the impingement axis and the highest at the outer edge of the disk. The interface temperature variation for constantan is also quite large due to its lower thermal conductivity. As the thermal conductivity increases, the thermal resistance within the solid becomes lower and the interface temperature becomes more uniform, as seen in the plots corresponding to copper and silicon. The crossover of the curves of the four materials and plain surface occurred due to a constant fluid flow and heat input rate that provides a constant thermal energy transfer for all circumstances. A narrow and elevated bell shape pattern is seen in Fig. 15 for solid materials with lower thermal conductivity. As the thermal conductivity is increased, a more uniform Nusselt number distribution is obtained.

One of the goals of this work was to develop a predictive trend of the average heat transfer coefficient. A correlation for the average Nusselt number was developed as a function of the thermal conductivity ratio, nozzle-to-target spacing, disk thickness, Ekman number, and Reynolds number to accommodate most of the transport characteristics of a confined liquid jet impingement cooling process. A correlation that best fit the numerical data can be placed in the following form:

$$Nu_{\text{av}} = 1.97619 \cdot \beta^{0.093} \cdot Re^{0.75} \cdot Ek^{-0.1111} \cdot (b/d_n)^{0.05} \cdot \varepsilon^{-0.69} \tag{19}$$

In developing this correlation, all average Nusselt number data corresponding to the variation of different parameters were used. Only data points corresponding to water as the fluid were used because the number of average heat transfer data points for other fluids was small. Figure 16 gives the comparison between the

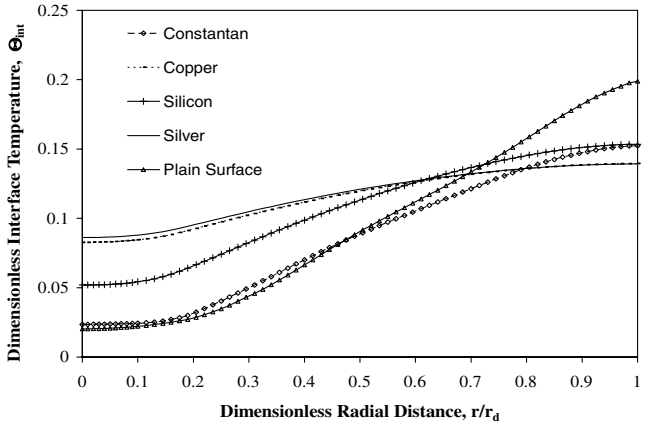

Fig. 14 Dimensionless interface temperature distributions for different solid materials with water as the cooling fluid ($Re = 1000$, $Ek = 4.25 \times 10^{-4}$, $\beta = 2.0$, $b/d_n = 0.25$).

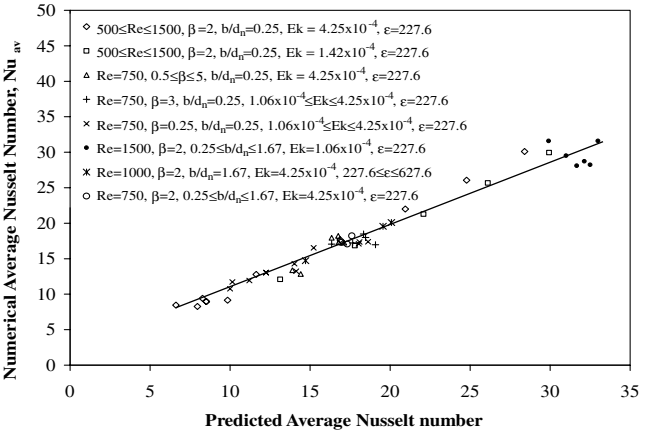

Fig. 16 Comparison of predicted average Nusselt numbers [Eq. (19)] with numerical data.

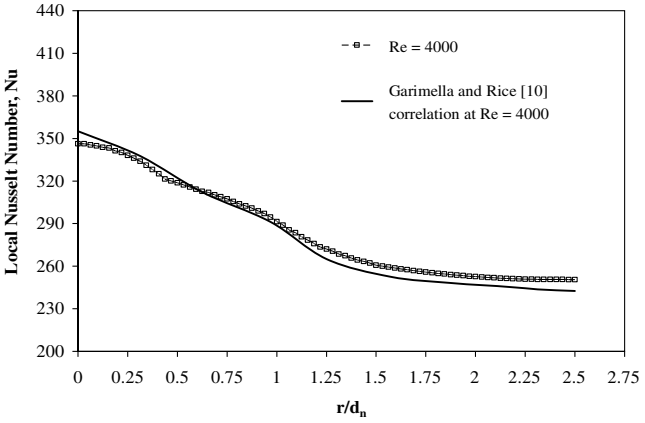

Fig. 17 Local Nusselt number distribution for a silver disk with FC-77 as the cooling fluid ($\beta = 4$, $Ek = \infty$).

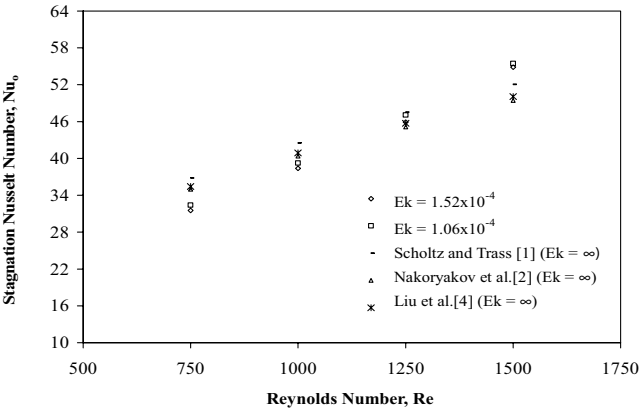

Fig. 18 Stagnation Nusselt number comparison of Scholtz and Trass [1], Nakoryakov et al. [2], and Liu et al. [4] with actual numerical results under different Reynolds and Ekman numbers ($d_n = 1.2$ mm, $b = 0.3$ mm).

numerical average Nusselt numbers to average Nusselt numbers predicted by Eq. (19). The average Nusselt number deviates in the range of -13.8 to $+15.3\%$ from that predicted by Eq. (19). The mean deviation is 6.8%. The ranges of the dimensionless variables used are as follows: $500 \le Re \le 1500$, $4.25 \times 10^{-5} \le Ek \le 1.06 \times 10^{-4}$, $0.25 \le \beta \le 5$, $Pr = 5.5$, $0.25 \le b/d_n \le 1.67$, $227.6 \le \varepsilon \le 627.6$. It should be noted from Fig. 16 that a large number of data points is very well correlated by Eq. (19). This correlation provides a convenient tool for the prediction of the average heat transfer coefficient under liquid jet impingement with a spinning confinement disk. The major difference between past studies and the present investigation is the accounting for conduction within the solid wafer and fluid for various materials, the spinning rate of the confinement disk, and the nozzle-to-target spacing ratio as a part of the correlation.

One of the papers used for the validation of this numerical study was the experimental work carried out by Garimella and Rice [10] using flouroinert FC-77 as the coolant. This liquid was tested for heat removal under a confined liquid jet impingement on a stationary disk. The confinement plate was also stationary ($Ek = \infty$). The simulation attempted to duplicate the exact conditions of that experiment. Figure 17 compares the variations of local Nusselt number distribution along the solid–fluid interface obtained from the simulation with the correlation developed from the experimental data. Considering the errors inherent in any experimental measurement (the reported uncertainty range of 0.13–3.2%) as well as discretization and round-off errors in the simulation, the comparison is quite satisfactory. Similar profiles have also been documented by Ma et al. [5].

Three other papers used for the validation of this numerical study were the analytical works carried out by Scholtz and Trass [1], Nakoryakov et al. [2], and Liu et al. [4] using fluids with a Prandtl number greater than unity as coolants. The fluids were tested for heat removal under a free liquid jet impingement on a heated flat surface maintained at uniform heat flux. The graphical representation of actual numerical Nusselt number results at the stagnation point at different Reynolds number are shown in Fig. 18. The results shown in Fig. 18 were on average within 8.17% of Scholtz and Trass [1], within 6.67% of Nakoryakov et al. [2], and within 6.75% of Liu et al. [4]. The local Nusselt number under Reynolds numbers of 750, 1000, 1250, and 1500 correlates with an average margin of 11.83, 6.31, 2.26, and 8.40%, respectively. Considering the inherent discretization and round-off errors, this comparison of the Nusselt number at the stagnation point is also quite satisfactory.

Conclusions

The solid–fluid dimensionless interface temperature and local Nusselt number showed a strong dependence on the Reynolds number, rotational rate, disk thickness, impingement height, fluid properties, and solid material properties. The increment of the Reynolds number increases the local heat transfer coefficient distribution values over the entire solid–fluid interface. In general, the rotational rate increases the local Nusselt number distribution values over the entire solid–fluid interface for $Ek > 1.52 \times 10^{-4}$. A thicker disk provides a more uniform distribution of the interface temperature and heat transfer coefficient. As the nozzle-to-target spacing increases from $\beta = 0.25$ to 1, the heat transfer coefficient decreases. However, at higher spacing ($\beta = 2$–5) a higher heat removal rate is obtained due to an optimal mix of the impinging jet flow with the rotationally induced flow. Higher Prandtl number fluids lead to a thinner thermal boundary layer and, therefore, a higher heat transfer coefficient at the interface. Plate materials with higher thermal conductivity maintained a lower thermal resistance within the solid and, therefore, more uniform temperature distribution results at the interface. Correlation for the average Nusselt number under spinning confined jet impingement cooling is proposed in terms of the Reynolds number, Ekman number, disk thickness, nozzle-to-target spacing, and thermal conductivity ratio. The differences between numerical and predicted values are in the range of -13.8 to $+15.3\%$. The mean value of the error is 6.8%. The numerical results compared reasonably well with available analytical predictions and experimental measurements.

References

[1] Scholtz, M. T., and Trass, O., "Mass Transfer in a Non-Uniform Impinging Jet: Part 1. Stagnation Flow Velocity and Pressure Distribution," *American Institute of Chemical Engineers Journal*, Vol. 16, No. 1, 1970, pp. 82–90. doi:10.1002/aic.690160117

[2] Nakoryakov, V. E., Pokusaev, B. G., and Troyan, E. N., "Impingement of an Axisymmetric Liquid Jet on a Barrier," *International Journal of Heat and Mass Transfer*, Vol. 21, No. 9, 1978, pp. 1175–1184. doi:10.1016/0017-9310(78)90136-9

[3] Womac, D. J., Ramadhyani, S., and Incropera, F. P., "Correlating Equations for Impingement Cooling of Small Heat Sources with Single Circular Liquid Jets," *Journal of Heat Transfer*, Vol. 115, No. 1, 1993, pp. 106–115.

[4] Liu, X., Lienhard, J. H., and Lombara, J. S., "Convective Heat Transfer by Impingement of Circular Liquid Jets," *Journal of Heat Transfer*, Vol. 13, No. 3, 1991, pp. 571–582.

[5] Ma, C. F., Sun, H., Auracher, H., and Gomi, T., "Local Convective Heat Transfer from Vertical Heated Surfaces to Impinging Circular Jets," *Proceedings of the Ninth International Heat Transfer Conference*, Vol. 2, Hemisphere, Washington, D.C., 1990, pp. 441–446.

[6] Garimella, S. V., and Nenaydykh, B., "Nozzle-Geometry Effects in Liquid Jet Impingement Heat Transfer," *International Journal of Heat and Mass Transfer*, Vol. 39, No. 14, 1996, pp. 2915–2923. doi:10.1016/0017-9310(95)00382-7

[7] Fitzgerald, J. A., and Garimella, S. V., "A Study of the Flow Field of a Confined and Submerged Impinging Jet," *International Journal of Heat and Mass Transfer*, Vol. 41, Nos. 8–9, 1998, pp. 1025–1034. doi:10.1016/S0017-9310(97)00205-6

[8] Li, D. Y., Guo, Z. Y., and Ma, C. F., "Relationship Between the Recovery Factor and the Viscous Dissipation in a Confined, Impinging, Circular Jet of High-Prandtl Number Liquid," *International Journal of Heat and Fluid Flow*, Vol. 18, No. 6, 1997, pp. 585–590. doi:10.1016/S0142-727X(97)00049-0

[9] Rahman, M. M., Dontaraju, P., and Ponnappan, R., "Confined Jet Impingement Thermal Management Using Liquid Ammonia as the Working Fluid," *Proceedings of International Mechanical Engineering Congress and Exposition*, American Society of Mechanical Engineers, Fairfield, NJ, 2002, pp. 1–10.

[10] Garimella, S. V., and Rice, R., "Confined and Submerged Liquid Jet Impingement Heat Transfer," *Journal of Heat Transfer*, Vol. 117, No. 4, 1995, pp. 871–877.

[11] Morris, G. K., and Garimella, S. V., "Orifice and Impingement Flow Fields in Confined Jet Impingement," *Journal of Electronic Packaging*, Vol. 120, No. 1, 1998, pp. 68–72.

[12] Li, C. Y., and Garimella, S. V., "Prandtl-Number Effects and Generalized Correlations for Confined and Submerged Jet Impingement," *International Journal of Heat and Mass Transfer*, Vol. 44, No. 18, 2001, pp. 3471–3480. doi:10.1016/S0017-9310(01)00003-5

[13] Ichimiya, K., and Yamada, Y., "Three-Dimensional Heat Transfer of a Confined Circular Impinging Jet with Buoyancy Effects," *Journal of Heat Transfer*, Vol. 125, No. 2, 2003, pp. 250–256. doi:10.1115/1.1527901

[14] Dano, B., Liburdy, J. A., and Kanokjaruvijit, K., "Flow Characteristics and Heat Transfer Performances of a Semi-Confined Impinging Array of Jets: Effect of Nozzle Geometry," *International Journal of Heat and Mass Transfer*, Vol. 48, Nos. 3–4, 2005, pp. 691–701. doi:10.1016/j.ijheatmasstransfer.2004.07.046

[15] Rahman, M. M., and Mukka, S. K., "Confined Liquid Jet Impingement on a Plate with Discrete Heating Elements," *Proceedings of the ASME Summer Heat Transfer Conference*, Vol. 4, American Society of Mechanical Engineers, Fairfield, NJ, 2005, pp. 637–647.

[16] Carper, H. J., Jr., and Deffenbaugh, D. M., "Heat Transfer from a Rotating Disk with Liquid Jet Impingement," *Proceedings of the Sixth International Heat Transfer Conference*, Vol. 4, Hemisphere, Washington D.C., 1978, pp. 113–118.

[17] Carper, H. J., Jr., Saavedra, J. J., and Suwanprateep, T., "Liquid Jet Impingement Cooling of a Rotating Disk," *Journal of Heat Transfer*, Vol. 108, No. 3, 1986, pp. 540–546.

[18] Metzger, D. E., Bunker, R. S., and Bosch, G., "Transient Liquid Crystal Measurements of Local Heat Transfer on a Rotating Disk with Jet Impingement," *Journal of Turbomachinery*, Vol. 113, No. 1, 1991, pp. 52–59.

[19] Thomas, S., Faghri, A., and Hankey, W. L., "Experimental Analysis and Flow Visualization of a Thin Liquid Film on a Stationary and Rotating Disk," *Journal of Fluids Engineering*, Vol. 113, No. 1, 1991, pp. 73–80.

[20] Rahman, M. M., and Faghri, A., "Numerical Simulation of Fluid Flow and Heat Transfer in a Thin Liquid Film over a Rotating Disk," *International Journal of Heat and Mass Transfer*, Vol. 35, No. 6, 1992, pp. 1441–1453. doi:10.1016/0017-9310(92)90035-Q

[21] Rahman, M. M., and Faghri, A., "Analysis of Heating and Evaporation from a Liquid Film Adjacent to a Horizontal Rotating Disk," *International Journal of Heat and Mass Transfer*, Vol. 35, No. 10, 1992, pp. 2655–2664. doi:10.1016/0017-9310(92)90106-3

[22] Saniei, N., Yan, X., and Schooley, W., "Local Heat Transfer Characteristics of a Rotating Disk Under Jet Impingement Cooling," *Proceedings of the Eleventh International Heat Transfer Conference*, Vol. 5, The Korean Society of Mechanical Engineers, Seoul, Republic of Korea, 1998, pp. 445–450.

[23] Saniei, N., and Yan, X., "Experimental Study of Heat Transfer from a Disk Rotating in an Infinite Environment Including Heat Transfer Enhancement by Jet Impingement Cooling," *Journal of Enhanced Heat Transfer*, Vol. 7, No. 4, 2000, pp. 231–245.

[24] Rahman, M. M., "Analysis of Simultaneous Gas Absorption and Chemical Reaction to a Thin Liquid Film over a Spinning Disk," *International Communications in Heat and Mass Transfer*, Vol. 27, No. 3, 2000, pp. 303–314. doi:10.1016/S0735-1933(00)00111-1

[25] Hung, Y. H., and Shieh, Y. R., "Convective Heat Transfer from a Rotating Ceramic-Based Multichip Disk with Round Jet Impingement," *Proceedings of the 35th National Heat Transfer Conference*, Vol. 1, American Society of Mechanical Engineers, Fairfield, NJ, 2001, pp. 97–103.

[26] Kang, H. S., and Yoo, J. Y., "Turbulence Characteristics of the Three-Dimensional Boundary Layer on a Rotating Disk with Jet Impingement," *Experiments in Fluids*, Vol. 33, No. 2, 2002, pp. 270–280.

[27] Shevchuk, I. V., Saniei, N., and Yan, X. T., "Impingement Heat Transfer over a Rotating Disk: Integral Method," *Journal of Thermophysics and Heat Transfer*, Vol. 17, No. 2, 2003, pp. 291–293.

[28] Iacovides, H., Kounadis, D., Launder, B. E., Li, J., and Xu, Z., "Experimental Study of the Flow and Thermal Development of a Row Cooling Jets Impinging on a Rotating Concave Surface," *Journal of Turbomachinery*, Vol. 127, No. 1, 2005, pp. 222–229. doi:10.1115/1.1812778

[29] Burmeister, L. C., *Convective Heat Transfer*, 2nd ed., Wiley, New York, 1993, Appendix C, pp. 581–590.

[30] Popiel, C. O., and Boguslawski, L., "Local Heat Transfer from a Rotating Disk in an Impinging Round Jet," *Journal of Heat Transfer*, Vol. 108, No. 2, 1986, pp. 357–364.

[31] Vanyo, J. P., "Rotating Fluids Applications," *Rotating Fluids in Engineering and Science*, 1st ed., Butterworth–Heinemann, MA, 1993, pp. 233–264.

[32] Özisik, M. N., *Heat Conduction*, 2nd ed., Wiley, New York, 1993, Appendix 1, pp. 657–660.

[33] Bejan, A., *Convection Heat Transfer*, 2nd ed., Wiley, New York, 1995, Appendix C, pp. 595–602.

[34] Fletcher, C. A. J., *Computational Galerkin Methods*, Springer–Verlag, New York, 1984, pp. 27 and 205.

[35] Ma, C. F., Zheng, Q., Lee, S. C., and Gomi, T., "Impingement Heat Transfer and Recovery Effect with Submerged Jets of Large Prandtl Number Liquid 2. Initially Laminar Confined Slot Jets," *International Journal of Heat and Mass Transfer*, Vol. 40, No. 6, 1997, pp. 1491–1500. doi:10.1016/S0017-9310(96)00070-1

[36] Brodersen, S., Metzger, D. E., and Fernando, H. J. S., "Flows Generated by the Impingement of a Jet on a Rotating Surface, Part 1: Basic Flow Patterns," *Journal of Fluids Engineering*, Vol. 118, No. 1, 1996, pp. 61–67.

[37] Hung, Y. H., and Lin, Z. H., "Effect of Confinement Plate on Heat Transfer Characteristics of a Circular Jet Impingement," *Fundamentals of Heat Transfer in Forced Convection*, HTD-Vol. 285, American Society of Mechanical Engineers, Fairfield, NJ, 1994, pp. 101–109.